Phase Behaviors of the $ZrMo_{2-x}W_xO_8$ (x = 0.2–2.0) System and the Preparation of an Mo-Rich Cubic Phase

Ling Huang,[a] Qiu-guo Xiao,[a] Hui Ma,[b] Guo-bao Li,[c] Fu-hui Liao,[c] Chuan-min Qi,[a] and Xin-hua Zhao*[a]

Keywords: Calorimetry / Materials science / Phase diagrams / Phase transitions / Zirconium

The phase behaviors of $ZrMo_{2-x}W_xO_8$ (x = 0.2 to 2.0) solid solutions have been studied systematically by variable-temperature X-ray diffraction (XRD) and differential scanning calorimetric (DSC) techniques. A low-temperature (LT) orthorhombic $ZrMo_{2-x}W_xO_8$ (x = 0.2–2.0) phase is formed by dehydration of the precursors $ZrMo_{2-x}W_xO_7(OH)_2(H_2O)_2$ (x = 0.2–2.0) within a temperature range from 124 to 203 °C. Among them, the orthorhombic $ZrMo_{2-x}W_xO_8$ solid solutions are able to convert further into metastable cubic phases within an x-dependent temperature range from 502 to 552 °C; the trigonal phases become dominant at higher temperature for Mo-rich solid solutions. However, no trigonal phases are formed in the high-temperature region for W-rich solid solutions. The absence of decomposition of $ZrMo_{2-x}W_xO_8$ (x = 0.2 to 1.6) solid solutions up to 800 °C indicates that the molybdenum substitution leads to a remarkable improvement of the thermal stability in comparison with ZrW_2O_8. Based on the phase behaviors reported in this paper, an approach for the preparation of cubic Mo-rich solid solutions $ZrMo_{2-x}W_xO_8$ with attractive negative thermal expansion (NTE) properties is demonstrated.

Introduction

The considerable interest in the study of cubic AM_2O_8 (A = Zr, Hf; M = W, Mo) compounds,[1–4] as well as their solid solutions $ZrMo_{2-x}W_xO_8$,[5–8] has been fueled recently by their isotropic negative thermal expansion (NTE) over a very wide temperature range. These compounds are usually synthesized by dehydration of the corresponding hydrate precursors. Typically, $ZrMo_2O_8$ and ZrW_2O_8 are obtained by dehydration of the precursors $ZrMo_2O_7(OH)_2(H_2O)_2$[9] and $ZrW_2O_7(OH)_2(H_2O)_2$,[10] respectively. The similarity in chemical and crystallographic properties between W^{VI} and Mo^{VI} suggests that the compounds ZrW_2O_8 and $ZrMo_2O_8$ should be isomorphic and readily form solid solutions. Solid solutions of $ZrMo_{2-x}W_xO_8$ have indeed been synthesized and the properties of $ZrMoWO_8$, including thermal expansion and oxygen migration at low temperature, have also been reported.[11] However, conspicuous gaps are seen with respect to the temperature-dependent phase behaviors of solid solutions of different compositions.

In this paper, the synthesis and phase behaviors of $ZrMo_{2-x}W_xO_8$ (x = 0.2–2.0) solid solutions are studied using variable-temperature X-ray diffraction (XRD) and different scanning calorimetric (DSC) techniques. It has been found that different structural phases of Mo-rich and W-rich $ZrMo_{2-x}W_xO_8$ solid solutions can be formed under the same heating conditions due to the differences in the thermal stabilities of ZrW_2O_8 and $ZrMo_2O_8$ polymorphs. Cubic, Mo-rich solid solutions of $ZrMo_{2-x}W_xO_8$ (x = 0.2, 0.4, 0.6, 0.7, 0.8) can be synthesized successfully by controlling the temperature within the appropriate range.

[a] Department of Chemistry, Beijing Normal University, Beijing, 100875, P. R. China
[b] Analyzing and Testing Center, Beijing Normal University, Beijing, 100875, P. R. China
[c] College of Chemistry and Molecular Engineering, Peking University, Beijing, 100871, P. R. China

Results and Discussion

Thermal Analysis

DSC curves were recorded in the temperature range of 40–800 °C for molybdenum-rich (x = 0.2, 0.4, 0.6, 0.7, or 0.8) and tungsten-rich (x = 1.0, 1.2, 1.4, 1.6, or 2.0) $ZrMo_{2-x}W_xO_7(OH)_2(H_2O)_2$ precursors. Typical DSC curves of the Mo-rich precursors $ZrMo_{1.6}W_{0.4}O_7(OH)_2(H_2O)_2$ and W-rich precursors $ZrMo_{0.4}W_{1.6}O_7(OH)_2(H_2O)_2$ are presented in Figure 1 (parts a and b), respectively. The single endothermic peak appearing in each of these curves (at 127 and 165 °C, respectively) indicates the formation of anhydrous orthorhombic phases due to dehydration in both cases. However, the DSC curve of the Mo-rich solid solution $ZrMo_{1.6}W_{0.4}O_8$ shows two exothermic peaks located at 508 and 562 °C assigned to the formation of a cubic and trigonal phase, respectively, although only one exothermic peak due to the formation of a cubic phase is observed at 542 °C in the DSC curve of the W-rich $ZrMo_{0.4}W_{1.6}O_8$ solid solu-

tion. This difference indicates clearly that there are two distinct phase-transition mechanisms operating during heating of Mo- and W-rich $ZrMo_{2-x}W_xO_8$ solid solutions.

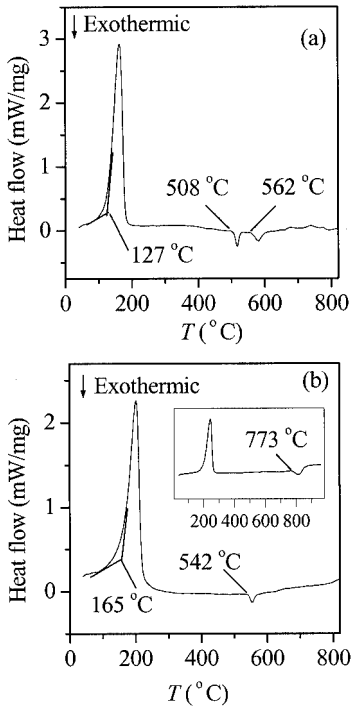

Figure 1. DSC curves of $ZrMo_{1.6}W_{0.4}O_7(OH)_2(H_2O)_2$ (a) and $ZrMo_{0.4}W_{1.6}O_7(OH)_2(H_2O)_2$ (b). The DSC of $ZrW_2O_7(OH)_2(H_2O)_2$, which indicates that ZrW_2O_8 decomposes at 773 °C, is given in the inset.

Increasing the tungsten fraction x leads to a gradual shift of the endothermic peak of the solid solutions $ZrMo_{2-x}W_xO_7(OH)_2(H_2O)_2$ (x = 0.2–2.0) from 124 up to 203 °C.

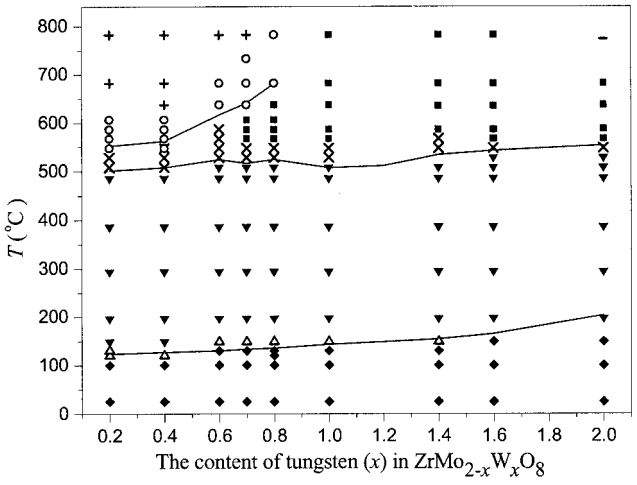

Figure 2. The overall process of phase transition for the $ZrMo_{2-x}W_xO_7(OH)_2(H_2O)_2$ system during the heating procedure. The solid lines link the onset peak values of the DSC curves. The crystal structures of precursor (black diamond) and dehydrates of specific composition x at different temperatures are indicated with different symbols: tetragonal: black diamond (♦); orthorhombic: black triangle (▼); tetragonal and orthorhombic: open triangle (Δ); orthorhombic and cubic: ×; cubic: black square (■); cubic and trigonal: open circle (○); trigonal: +; decomposition: –.

Similarly, the increase in x also causes an up-shift of the first exothermic peak from 502 to 552 °C. However, the second exothermic peak of $ZrMo_{2-x}W_xO_8$ ($1 \leq x < 2$) disappears at higher temperature, although it shows a more remarkable shift for solid solutions $ZrMo_{2-x}W_xO_8$ with x less than 1.0 (see Figure 2). The appearance of the exothermic peak in the DSC curve of ZrW_2O_8 suggests its decomposition temperature is located at 773 °C (see the inset in Figure 1, b). This observation indicates that these solid solutions have a higher decomposition temperature than ZrW_2O_8. A similar feature has been observed for the $ZrMo_{2-x}W_xO_8$ solid solution.[6] In addition, no enthalpy changes due to MoO_3 sublimation of $ZrMo_{2-x}W_xO_8$ compounds (x = 0.2–1.6) are detected at temperatures up to 800 °C even though MoO_3 sublimation has been reported to occur for $ZrMo_2O_8$ at 750 °C.[4]

Variable-Temperature XRD Analysis

The composition- and temperature-dependence of the phase behaviors of $ZrMo_{2-x}W_xO_7(OH)_2(H_2O)_2$ solid solutions were examined by variable-temperature XRD measurement in real time as they are expected to indicate the mechanism responsible for the phase transition detected by the DSC measurements. Figures 3 and 4 show the variable-temperature XRD patterns of $ZrMo_{1.6}W_{0.4}O_7(OH)_2(H_2O)_2$ and $ZrMo_{0.4}W_{1.6}O_7(OH)_2(H_2O)_2$, respectively. Based on refined XRD patterns of $ZrMo_{2-x}W_xO_7(OH)_2(H_2O)_2$, it is evident that precursors at the temperature below the endothermic peak exist in the form of a tetragonal phase. As demonstrated by the typical XRD patterns of $ZrMo_{1.6}W_{0.4}O_8$ in the temperature range 120–508 °C and $ZrMo_{0.4}W_{1.6}O_8$ in the temperature range 197–567 °C, all $ZrMo_{2-x}W_xO_8$ solid solutions (x = 0.2–2.0) formed by precursor dehydration show XRD patterns similar to that observed for o-$ZrMo_{0.4}W_{1.6}O_8$.[12] Hence, the XRD patterns of all $ZrMo_{2-x}W_xO_8$ solid solutions can be indexed using the orthorhombic structure of o-$ZrMo_{0.4}W_{1.6}O_8$ with the space group $Pmn2_1$ as reference; the indexed results are summarized in Table 1.

A close inspection of the XRD pattern of $ZrMo_{1.6}W_{0.4}O_7(OH)_2(H_2O)_2$ collected at 120 °C (Figure 3) reveals a shoulder diffraction peak located at 21° (2θ), which seems to be assignable to the 111 diffraction of o-$ZrMo_{1.6}W_{0.4}O_8$. The appearance of this shoulder indicates the beginning of the dehydration of the $ZrMo_{1.6}W_{0.4}O_7(OH)_2(H_2O)_2$ precursor; this dehydration process is complete at around 149 °C, as demonstrated by the disappearance of the XRD pattern of the hydrate precursor at this temperature. The accompanied enhancement and sharpening of the XRD peaks upon increasing the temperature from 149 to 486 °C illustrates that o-$ZrMo_{1.6}W_{0.4}O_8$ grows subsequently to the fine crystal. Combing the XRD patterns with the DSC curves displayed in Figure 2 shows that the o-$ZrMo_{1.6}W_{0.4}O_8$ phase converts into the cubic phase c-$ZrMo_{1.6}W_{0.4}O_8$ at 508 °C, which converts, in turn, into the thermodynamically stable trigo-

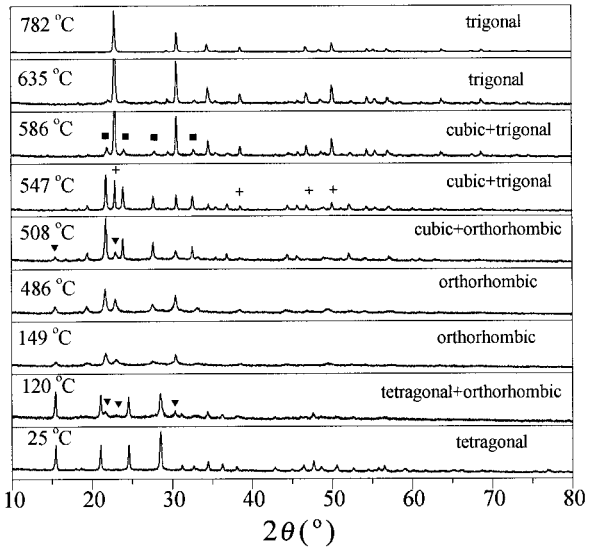

Figure 3. The variable-temperature XRD patterns of $ZrMo_{1.6}W_{0.4}O_7(OH)_2(H_2O)_2$ (25 °C) and $ZrMo_{1.6}W_{0.4}O_8$. The diffraction peaks characterizing the polymorphs are marked by a black triangle (▼) (orthorhombic), a black square (■) (cubic), or (+) (trigonal). The denoted temperatures were calibrated against KCl.

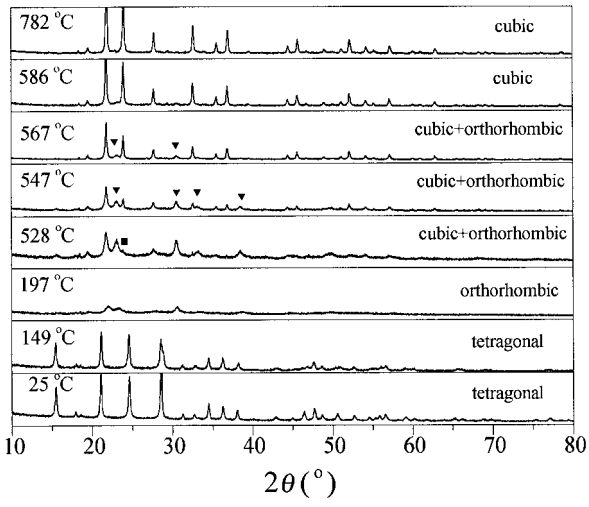

Figure 4. The variable-temperature XRD patterns of $ZrMo_{0.4}W_{1.6}O_7(OH)_2(H_2O)_2$ (≤149 °C) and $ZrMo_{0.4}W_{1.6}O_8$. The diffraction peaks characterizing the polymorphs are marked by a black triangle (▼) (orthorhombic) or a black square (■) (cubic). The denoted temperatures were calibrated against KCl.

nal phase within a narrower temperature "window" of about 54 °C (508–562 °C) at the expense of formation of a pure cubic phase. Therefore, the pure cubic phases of Mo-rich solid solutions can be formed only under carefully controlled temperature conditions.

The pure trigonal $ZrMo_{2-x}W_xO_8$ (x = 0.2–0.7) was prepared at 782 °C and was indexed by using the α′-$ZrMo_2O_8$ model of space group $P\bar{3}m1$[13] rather than α-$ZrMo_2O_8$ of space group $P\bar{3}1c$,[14] because of the absence of 201, 103, and 211 diffractions in the XRD pattern of trigonal $ZrMo_{1.6}W_{0.4}O_8$. The pure trigonal phases of $ZrMo_{2-x}W_xO_8$ (x = 0.2–0.7) are thermodynamically stable up to 800 °C; their lattice parameters are summarized in Table 2.

Table 1. Lattice parameters of o-$ZrMo_{2-x}W_xO_8$ solid solutions at 386 °C.

x	a [Å]	b [Å]	c [Å]	V [Å^3]
0.2	5.86	7.33	9.13	392
0.4	5.86	7.34	9.15	393
0.6	5.86	7.25	9.12	387
0.7	5.86	7.24	9.12	387
0.8	5.85	7.23	9.11	386
1.0	5.85	7.24	9.10	386
1.2	5.85	7.23	9.10	385
1.4	5.85	7.22	9.10	384
1.6	5.85	7.21	9.11	384
2.0	5.85	7.21	9.10	384

Table 2. The lattice parameters of the trigonal phase of $ZrMo_{2-x}W_xO_8$ (x = 0.2–0.7) solid solutions at 782 °C.

x	a [Å]	c [Å]	V [Å^3]
0.2	5.824	6.051	177.7
0.4	5.833	6.075	178.9
0.6	5.825	6.040	177.4
0.7	5.823	6.036	177.3

The stability of cubic $ZrMo_{2-x}W_xO_8$ solid solutions (x = 0.2–0.8) increases rapidly with increasing W-fraction (x) from 0.2 to 0.8. As indicated in Figure 2, the metastable pure cubic phases of the solid solutions of x = 0.7 and 0.8 exist over a wide temperature range, and when x is greater than or equal to 1.0 the metastable cubic phase can be found even at temperature up to 800 °C.

Figure 4 indicates that the W-rich solid solution $ZrMo_{0.4}W_{1.6}O_7(OH)_2(H_2O)_2$ converts completely into orthorhombic o-$ZrMo_{0.4}W_{1.6}O_8$ at 197 °C, which is stable up to 528 °C. This observation suggests that the orthorhombic isomorphs of W-rich solid solutions appear to be more stable than those of Mo-rich solid solutions.

The appearance of the small peak located at about 23.8° (2θ) due to the 211 diffraction of the cubic phase in the XRD pattern collected at 528 °C indicates further that W-rich o-$ZrMo_{2-x}W_xO_8$ solid solutions, including o-$ZrMo_{0.4}W_{1.6}O_8$, convert into a cubic phase at 528 °C and that these cubic phases, except x = 2.0, are stable at temperatures up to 782 °C. Since the 310 diffraction of 31° (2θ) disappears at this temperature, the cubic phase can be assigned to the structure type β-ZrW_2O_8. This feature is true for all W-rich solid solutions.

Phase Behaviors of Solid Solutions

Figure 2 displays the phase-transition processes of $ZrMo_{2-x}W_xO_7(OH)_2(H_2O)_2$ solid solutions deduced on the basis of the XRD and DSC experiments outlined above. It can be seen that decomposition of the precursors proceeds through a sequential phase-transition process, namely tetragonal → orthorhombic → cubic → trigonal polymorphs. The phase-transition temperatures increase with increasing

W-fractions. This dependence is understandable in terms of the bond strength of W–O, which is stronger than that of Mo–O (the bond-dissociation energies for these bonds are 672.0 ± 41.8 and 560.2 ± 20.9 kJ mol^{-1}, respectively).[15]

The difference in phase-transition mechanism of W-rich and Mo-rich solid solutions can be interpreted in terms of trigonal phase formation. Cubic ZrW_2O_8 is metastable over a wide temperature range below 777 °C, whereas the cubic phase of $ZrMo_2O_8$ is dynamically stable only over a narrower window ranging from 480 to 520 °C, above which trigonal $ZrMo_2O_8$ crystallizes.[4] So, it would be expected that the stability of cubic phases of $ZrMo_{2-x}W_xO_8$ solid solutions at high temperature would be greater for W-rich $ZrMo_{2-x}W_xO_8$ solid solutions due to prevention of trigonal phase formation. A close inspection of the phase-composition dependence of behaviors for the $ZrMo_{2-x}W_xO_8$ solid solution reveals indeed that a dynamic equilibrium between these two processes can be established at $x = 1.0$, above which, i.e. $1 \leq x < 2$, the cubic phase is stable at temperatures up to 800 °C; however, the stable cubic phase is difficult to form in solid solutions of $x \leq 0.8$ in the same temperature range.

It is of interest to note that the stability of $ZrMo_{2-x}W_xO_8$ solid solutions can be improved by increasing the Mo fraction. In this way, the decomposition of this solid solution to the corresponding oxides can be prevented even at 800 °C. Therefore, as compared to both ZrW_2O_8 and $ZrMo_2O_8$, $ZrMo_{2-x}W_xO_8$ solid solutions appear to be more stable due to the entropy effect induced by W or Mo doping. Moreover, $ZrMo_{2-x}W_xO_8$ ($1 \leq x \leq 1.6$) solid solutions show a lower phase-transition temperature and have negative expansion coefficients; they are also stable over a wider temperature range. All these factors make solid solutions of this kind more attractive for use in optical and electronic devices.

Preparation of an Mo-Rich $ZrMo_{2-x}W_xO_8$ Solid Solution of a Pure Cubic Phase

Variable-temperature XRD measurements of $ZrMo_{2-x}W_xO_8$ in real time demonstrate that the yield for the orthorhombic → cubic as well as the cubic → trigonal phase-transition depends not only on the system composition and temperature, but also on the temperature-holding time. Hence, strict control of both the temperature and temperature-holding time are crucial for preparation of an Mo-rich cubic phase. The pure cubic phase of $ZrMo_2O_8$ has been synthesized by Lind[4] under rigorously controlled experimental conditions. Following the thermal phase-transition process formulated on the basis of our DSC and XRD data outlined above, we have successfully prepared a pure cubic phase of Mo-rich solid solutions $ZrMo_{2-x}W_xO_8$ with $x = 0.4$, 0.6 and 0.7, 0.8 by holding the temperature at 520 and 530 °C, respectively, for 2 h, followed by rapid cooling to room temperature. It should be noted that a higher temperature is able to accelerate the trigonal phase formation. In addition, a pure cubic phase of $x = 0.2$ cannot be formed in this way, although it can be prepared by two-step heating, i.e. by heating at 365 °C for 12 h and then 5 h at 450 °C. The cubic phases prepared under such conditions do not show a 310 (30.9°) diffraction, and hence are assignable to crystalline β-ZrW_2O_8 type structure, for which the indexed pattern is displayed in Figure 5; lattice parameters of c-$ZrMo_{2-x}W_xO_8$ ($x = 0.2$, 0.4, 0.6, 0.7, and 0.8) are listed in Table 3.

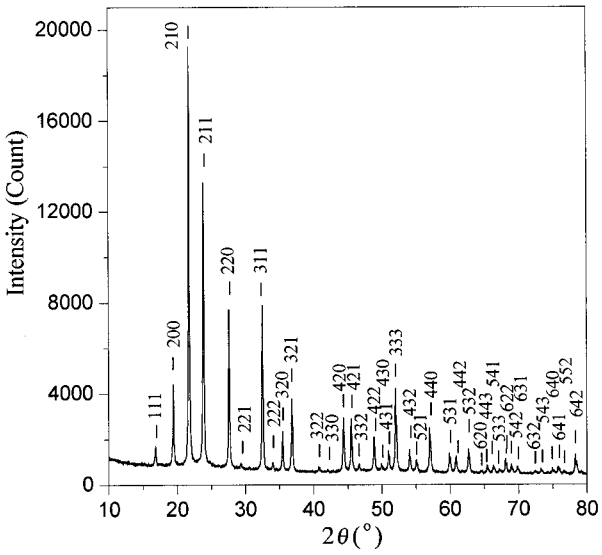

Figure 5. The indexed X-ray diffraction pattern for c-$ZrMo_{1.6}W_{0.4}O_8$.

Table 3. Lattice parameters of c-$ZrMo_{2-x}W_xO_8$ ($x = 0.2$, 0.4, 0.6, 0.7, and 0.8).

x	a [Å]
0.2	9.1311(1)
0.4	9.1312(1)
0.6	9.1311(2)
0.7	9.1318(9)
0.8	9.1317(1)

Conclusions

The precursors $ZrMo_{2-x}W_xO_7(OH)_2(H_2O)_2$ ($x = 0.2$–2.0) are converted into a $ZrMo_{2-x}W_xO_8$ orthorhombic phase within an x-dependent temperature range from 124 to 203 °C by removal of three water molecules. The temperature dependence of $ZrMo_{2-x}W_xO_8$ shows two types of phase behavior: the orthorhombic phases of Mo-rich $ZrMo_{2-x}W_xO_8$ ($x = 0.2$–0.8) are able to convert into trigonal phases, with cubic phase formation as the intermediate step, and the metastable pure cubic phases can be prepared by carefully controlling the temperature and temperature-holding time in the appropriate temperature range. However, no trigonal phases can be formed in the W-rich solid solutions $ZrMo_{2-x}W_xO_8$ ($x = 1.0$–1.6). In addition, the solid solutions of this type do not decompose even at temperatures up to 800 °C, even though the decomposition

temperature of ZrW_2O_8 is 773 °C. Therefore, doping of tungsten into cubic $ZrMo_2O_8$ increases its stability towards decomposition.

Experimental Section

Preparation and Characterization of $ZrMo_{2-x}W_xO_7(OH)_2(H_2O)_2$ Precursors: Precursors $ZrMo_{2-x}W_xO_7(OH)_2(H_2O)_2$ were prepared following procedures described previously.[5,7] Briefly, the reactants $Na_2WO_4{\cdot}2H_2O$, $Na_2MoO_4{\cdot}2H_2O$, and $ZrOCl_2{\cdot}8H_2O$ (A.R. grade) were first heated at 800 °C for 6 h and the exact hydration number was re-determined based on the water loss. Dropwise addition of 50 mL of an aqueous solution of 0.5 M Zr^{4+}, together with 50 mL of an aqueous solution of 1 M mixed ionic solution [W^{6+} + Mo^{6+}] with different x (x = 0.2, 0.4, 0.6, 0.7, 0.8, 1.0, 1.2, 1.4, 1.6, or 2.0), into 30 mL of distilled water led to immediate formation of a white precipitate. The white turbid solution formed was then mixed with 182 mL of 6 M aqueous HCl solution with continuous stirring for 4 h and then refluxed for 48 h. The white precipitate was finally separated by centrifugation and washed sequentially with 1.5 M aqueous HCl and distilled water. The obtained products were confirmed to have the desired Zr to W/Mo ratios as indicated by the negligible amounts (<1%) of these ions in the decanted liquid determined by ICP-AES (JY, ULTIMA, France).

The hydration number of the precursors $ZrMo_{2-x}W_xO_7(OH)_2(H_2O)_2$ was estimated from the weight-loss percentage of the dried white precipitate measured by TG (Netzsch Sta 409C).

The refined XRD pattern of $ZrMo_{1.6}W_{0.4}O_7(OH)_2(H_2O)_2$, as a typical example, is shown in Figure 6; it indicates that all white or slightly pale $ZrMo_{2-x}W_xO_7(OH)_2(H_2O)_2$ powders are isomorphs of tetragonal $ZrMo_2O_7(OH)_2(H_2O)_2$. The final refinement results are listed in Table 4.

DSC Measurements: DSC curves in the temperature range 40–800 °C were recorded with a DTA-404 PC (Netzsch), under argon, at a heating rate of 10 °C min^{-1}; an empty crucible was used as the reference. The DSC curve of the samples was calibrated using those recorded for a pair of blank platinum crucibles under the same conditions. The peak temperatures were calibrated using the metals In, Sn, Bi, Zn, Al, Ag, Au, and Ni as standard substances and the precision was estimated to be ±1 °C.

X-ray Crystallographic Equipment and Temperature Calibration: The XRD patterns were collected on a Philips X′-Pert MPD diffractometer with X′Celerator detector using Cu-K_α radiation (40 kV, 40 mA). Each ground sample was mounted on a platinum strip, which served as sample holder as well as heater attached with Anton Parr high-temperature units used for variable temperature XRD measurements. The routine XRD patterns were collected within the 2θ range 10–120° with a step width of 0.0167° (2θ) and

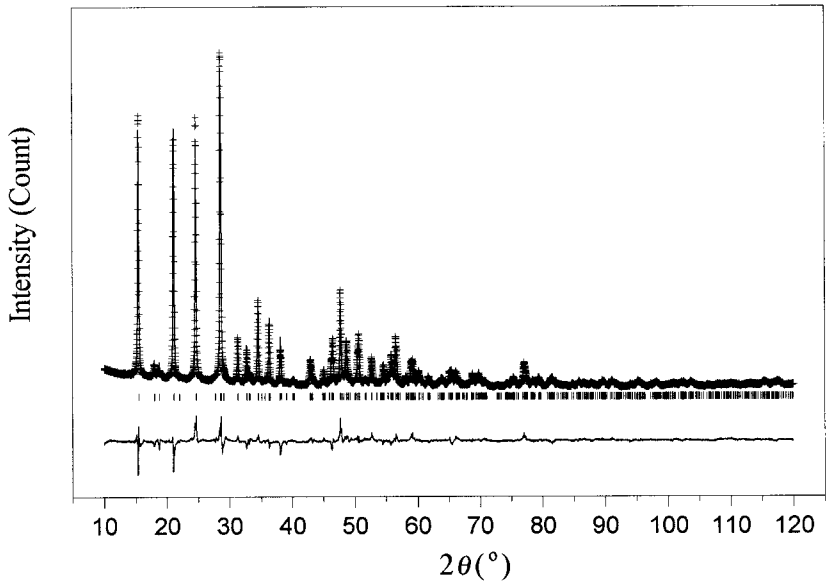

Figure 6. Experimental, calculated, and difference X-ray diffraction patterns for $ZrMo_{1.6}W_{0.4}O_7(OH)_2(H_2O)_2$.

Table 4. The crystal structural parameters of $ZrMo_{2-x}W_xO_7(OH)_2(H_2O)_2$ refined using Rietveld method.

x	a [Å]	c [Å]	v [Å^3]	Zr (8a: 0,0,z)	W/Mo (16b: x,y,z)	Rp [%]	Rwp [%]
0.2	11.443(9)	12.492(1)	1635.9	–0.0071(1)	0.0173(2), 0.1626(2), 0.2255(1)	7.75	10.78
0.4	11.4460(3)	12.4861(4)	1635.8	–0.0037(3)	0.0176(2), 0.1644(2), 0.2291(3)	5.95	7.81
0.6	11.441 (2)	12.482(2)	1633.8	–0.0079(6)	0.0177(2), 0.1642(1), 0.2283(6)	5.98	7.80
0.7	11.436(2)	12.474(2)	1631.4	–0.0086(7)	0.0174(2), 0.1641(2), 0.2289(7)	6.29	7.95
0.8	11.435(2)	12.474(2)	1631.1	–0.0060(7)	0.0180(2), 0.1664(2), 0.2282(7)	5.93	7.98
1.0	11.431(2)	12.468 (4)	1629.4	–0.0106(8)	0.0165(2), 0.1637(1), 0.2275(7)	5.95	7.80
1.2	11.429(2)	12.470(3)	1628.9	–0.0103(9)	0.0147(2), 0.1625(2), 0.2298(8)	7.16	9.47
1.4	11.436(2)	12.473(2)	1631.4	–0.0104(9)	0.0152(2), 0.1635(1), 0.2267(8)	6.39	8.39
1.6	11.432(2)	12.475(2)	1630.4	–0.0128(9)	0.0146(2), 0.1638(1), 0.2268(9)	7.10	9.21
1.6[12]	11.4245(5)	12.4619(7)	1625.5	–0.0140(2)	0.0167(2), 0.1638(2), 0.2223(3)	7.12	8.79
2.0	11.4432(4)	12.4865(5)	1635.1	–0.0053(9)	0.0186(1), 0.1646(1), 0.2297(8)	9.76	12.62

step time of 20 s, whereas the variable temperature XRD patterns were recorded within the 2θ range 10–80° with the same step width and a step time of 30 s. The measurements were carried out under argon at temperatures at which the possible phase transition was suggested to occur according to the DSC data. The heating rate between two neighboring temperature was about 2 °C min^{-1} and at each point the temperature was held for 20 min. The temperatures during the measurement were controlled with a TCU 2000 unit and were calibrated using an interpolation technique based on the Pathak equation[16] with KCl as the external standard.

The observed profiles of the XRD patterns for the precursors were refined using the Rietveld method contained in the GSAS program[17] by fitting to tetragonal $ZrMo_2O_7(OH)_2(H_2O)_2$[8] as the model. The refinement was started with lattice parameters and atomic coordinates assigned from the model. The site fraction of Mo/W atom was fixed as the intended ratio according to the precursor formula. The fitting was carried out for the lattice parameters, the scale parameters, background coefficients, and profile coefficients. Finally, the atomic coordinates and the isotropic thermal factors of metals (Zr, Mo, W) were refined.

Analysis and indexing of the XRD patterns for $ZrMo_{2-x}W_xO_8$ were performed using the PowderX program.[18] The zero-point shifts was corrected using the line-pair method. SiO_2 was used as an internal standard to correct the XRD peak positions used to calculate the precise lattice parameters of cubic $ZrMo_{2-x}W_xO_8$.

Acknowledgments

Support for this research from the National Science Foundation of China under grants NSFC 20471010 and 20371009 and the Foundation of Beijing Key Discipline of Inorganic Chemistry of Beijing Education Committee are gratefully acknowledged.

[1] T. A. Mary, J. S. O. Evans, T. Vogt, A. W. Sleight, *Science* **1996**, *272*, 90–92.
[2] J. S. O. Evans, T. A. Mary, T. Vogt, M. A. Subramanian, A. W. Sleight, *Chem. Mater.* **1996**, *8*, 2809–2823.
[3] C. Lind, A. P. Wilkinson, Z. Hu, S. Short, J. D. Jorgensen, *Chem. Mater.* **1998**, *10*, 2335–2337.
[4] C. Lind, A. P. Wilkinson, C. J. Rawn, E. A. Payzant, *J. Mater. Chem.* **2001**, *11*, 3354–3359.
[5] C. Closmann, A. W. Sleight, J. C. Haygarth, *J. Solid State Chem.* **1998**, *139*, 424–426.
[6] U. Kameswari, A. W. Sleight, J. S. O. Evans, *Int. J. Inorg. Mater.* **2000**, *2*, 333–337.
[7] S. Zhang, X. Zhao, H. Ma, X. Wu, *Chin. J. Chem.* **2000**, *18*, 571–575.
[8] J. S. O. Evans, P. A. Hanson, R. M. Ibberson, N. Duan, U. Kameswari, A. W. Sleight, *J. Am. Chem. Soc.* **2000**, *122*, 8694–8699.
[9] A. Clearfield, R. H. Blessing, *J. Inorg. Nucl. Chem.* **1972**, *34*, 2643–2663.
[10] A. Clearfield, R. H. Blessing, *J. Inorg. Nucl. Chem.* **1974**, *36*, 1174–1176.
[11] S. Allen, J. S. O. Evans, *J. Mater. Chem.* **2004**, *14*, 151–156.
[12] X. Zhao, L. Huang, P. Liu, H. Ma, *Chin. J. Chem.* **2003**, *21*, 1529–1531.
[13] S. Allen, R. J. Ward, M. R. Hampson, R. K. B. Gover, J. S. O. Evans, *Acta Crystallogr., Sect. B* **2004**, *60*, 32–40.
[14] M. Auray, M. Quarton, P. Tarte, *Acta Crystallogr., Sect. C* **1986**, *42*, 257–259.
[15] D. R. Lide, *CRC Handbook of Chemistry and Physics*, CRC Press Ltd., Boca Raton, Florida, **2001**.
[16] P. D. Pathak, N. G. Vasavada, *Acta Crystallogr., Sect. A* **1970**, *26*, 655–658.
[17] A. C. Larson, V. Dreele, R. B. Lansce, Los Alamos National Lab, Los Alamos, NM, **1994**.
[18] C. Dong, *J. Appl. Crystallogr.* **1999**, *32*, 838.

Received: May 30, 2005
Published Online: October 11, 2005

